Journal of Cluster Science (2023) 34:1819–1829
https://doi.org/10.1007/s10876-022-02345-z

ORIGINAL PAPER

Pt Nanoparticles Incorporated $Znfe_2o_4$ Nanoparticles Supported on Hollow Poly(aniline-co-pyrrole)/Chitosan as a Novel Catalyst for Methanol Oxidation

Iran Bameri[1] · Jilla Saffari[2] · Mehri-Saddat Ekrami-Kakhki[3] · Sahar Baniyaghoob[1]

Received: 22 May 2022 / Accepted: 12 August 2022 / Published online: 19 September 2022

Abstract
In this work, hollow Poly(aniline-co-pyrrole) (HAP) nanoparticles were synthesized and utilized accompanied by chitosan (CH) to prepare the novel HAP-CH support for metal nanoparticles. $ZnFe_2O_4$ (ZFO) nanoparticles were synthesized and incorporated on HAP-CH support to enhance the catalytic activity of Pt nanoparticles in the novel Pt-ZFO/HAP-CH nanocatalyst for methanol electro-oxidation. The prepared catalysts were characterized by Transmission electron microscopy images, Fourier-transform infrared spectroscopy, energy dispersive X-ray, and X-ray powder diffraction analysis. The electrocatalytic performance of Pt-ZFO/HAP-CH nanocatalyst was assessed towards methanol electro-oxidation by some electrochemical techniques including electrochemical impedance spectroscopy, chronoamperometry, and cyclic voltammetry, and compared with that of Pt/HAP-CH. Electrochemical results illustrated that Pt-ZFO/HAP-CH nanocatalyst has higher electrocatalytic activity and durability than that of the Pt/HAP-CH, which is owing to the higher electrochemically active surface area, higher mass activity, better durability, and lower charge transfers resistance. The superior catalytic performance of Pt-ZFO/HAP-CH nanocatalyst reveals that it can be a promising catalyst for developing direct methanol fuel cells (DMFCs).

Keywords Chitosan · Methanol electro-oxidation · Poly(aniline-co-pyrrole) · $ZnFe_2O_4$

Introduction

Consumption of energy is swiftly increasing because of population growth, technological development, and industrialization [1, 2]. Apart from the growing energy demand, fossil energy reserves are also quickly decreasing. On the other hand, natural environment destruction is another threat [3]. Recently, sustainable, eco-friendly, and renewable sources like fuel cells have been receiving great attention, rather than fossil energy resources that their reserves are declining [4, 5]. Fuel cells are very versatile. They can operate with a wide range of fuels, electrolytes, and oxidants and they possess large energy conversion efficiency [6, 7]. Liquid fuel cells paid extensive research fascinates in recent years. Direct methanol fuel cells (DMFCs) are regarded as one of the superb power sources owing to the methanol fuel availability, low pollutant emission, high energy conversion efficiency, simple system, and low operating temperature [8, 9]. However, their satisfactory commercial application on large scale is still intensely impeded by a number of technical shortfalls, particularly the unfavorable durability and activity troubles of catalysts for methanol oxidation (MO). Likewise, fabricating affordable catalysts with high activity for electro-oxidation of methanol is a great goal for DMFCs' development. To fulfill the commercialization of DMFCs, it is necessary to have highly effective, stable, highly active, and inexpensive catalysts for the methanol oxidation reaction (MOR) [10, 11].

Platinum (Pt) is known as an efficient catalyst for methanol electro-oxidation in fuel cells, and plenty of studies have been accomplished on Pt and Pt-based materials [12, 13]. However, the CO poisoning effect, slow MOR kinetics, and high cost are the major disadvantages of Pt-based catalysts, therefore impeding their commercial

✉ Jilla Saffari
saffarijilla@gmail.com

1 Department of Chemistry, Science and Research Branch, Islamic Azad University, Tehran, Iran

2 Department of Chemistry, Zahedan Branch, Islamic Azad University, P.O. Box 98135-978, Zahedan, Iran

3 Central Research Laboratory, Esfarayen University of Technology, Esfarayen, North Khorasan, Iran

applications [14, 15]. Hence, the design and synthesis of an electrocatalyst with high catalytic activity, great long-term stability, and high tolerance versus poisonous intermediate remains a great challenge for scientists in this field.

To diminish the poisoning effects of CO_{ads} in MOR, it is necessary to develop efficient electrocatalysts that can provide plentiful oxygenated species. For example, hydroxyl species (OH_{ads}) are proper candidates for the oxidation of CO_{ads} intermediates. To this end, a number of approaches have been reported like the modification and creation of Pt electrocatalysts via combining them with transition metals or the rest of noble metals, like Co, Ni, Pd, Ru, or even doped them with other non-metals [16–18]. Recent studies on transition metal mixed oxides with a large number of oxygen vacancies and high electrical conductivities have illustrated that they have great potential to utilize in fuel cells rather than noble metals.

In recent years, perovskite substances were presented as encouraging candidates in photocatalytic, storage [19], energy conversion, and sensor applications [20]. Perovskites are oxides with a standard formula of ABO_3, B refers to transition metal possessing a small radius cation, and A represents rare earth or alkaline earth metal with a rather larger radius cation [21]. They have significant catalytic activity for plenty of reactions. Compared to single oxides, perovskites have advantages such as high structural, thermal, and chemical stability. The chief features of perovskites are mixed ionic and electronic conducting behavior, and oxygen sorption properties, high oxygen mobility within their lattice [22].

Besides, it has established fact that electrocatalysis is an effect of the surface, and choosing an appropriate supporting catalyst substance can affect the electrochemical efficiency of the supported electrocatalysts because of the interaction and surface reactivity. Throughout the last years, using (bio)-polymers like polypyrrole (PPy) [23], polythiophene (PTh) [24], polyaniline (PANI) [25], and chitosan (CH) [26] has sparked a great deal of attention because of their broad diversity of electro-conductive and physical characteristics.

By taking mentioned advantages, in this study, the novel hollow Poly(aniline-co-pyrrole)-chitosan was prepared and utilized as support for Pt nanoparticles. $ZnFe_2O_4$ perovskite nanoparticles were used accompanied by Pt nanoparticles to prepare the novel Pt-ZFO/HAP-CH catalyst. The catalytic performance of the synthesized catalyst was assessed for methanol electro-oxidation and compared with Pt/HAP-CH catalyst. The catalytic performance of the synthesized Pt-ZFO/HAP-CH catalyst was evaluated for methanol oxidation by several electrochemical techniques, such as electrochemical impedance spectroscopy (EIS), chronoamperometry (CA), and cyclic voltammetry (CV).

Experimental

Materials

Iron (III) nitrate nonahydrate ($Fe(NO_3)_3{\cdot}9H_2O$), zinc chloride ($ZnCl_2$), sodium hydroxide (NaOH), octanoic acid, chloroplatinic acid hexahydrate ($H_2PtCl_6{\cdot}6H_2O$), $NaBH_4$ (96%), aniline, pyrrole, sulfuric acid (H_2SO_4, 98%), acetic acid 1%, ammonium persulfate (APS [$(NH_4)_2S_2O_8$, 98%]) and methanol (CH_3OH, 99.2%) were purchased from Merck. Chitosan (low molecular weight) and TX -100 were purchased from Sigma-Aldrich.

Physicochemical Characterization

To characterize the functional groups and structures of the samples, Fourier Transmission Infrared (FT-IR, Rayleigh-WQF-510A) was utilized. The crystallite nature of the samples was corroborated by X-ray diffractometry (XRD, Philips X' Pert Pro, Netherlands) applying CuK_α radiation (k = 1.54178 Å). EDX detector (IE 300X, Oxford, UK) attached to SEM was used to analyze the elemental composition of materials. Transmission electron microscopy (TEM) images were taken by an LEO 912 AB microscope to identify the morphology of the catalysts. The magnetic characteristic of as-prepared catalysts was analyzed utilizing vibrating sample magnetometry (VSM, AGFM Meghnatis Daghigh Kavir Co., Kashan, Iran). The inductively coupled plasma optical emission spectroscopy (ICP-OES, Shimadzu ICPE-9800 spectrometer) was utilized to determine the amount of Pt nanoparticles, loaded on the working electrodes' surface.

Synthesis of $ZnFe_2O_4$ (ZFO) Nanoparticles

First, 0.01 mol of $ZnCl_2$ and 0.01 mol of $Fe(NO_3)_3{\cdot}9H_2O$ were separately dissolved in 10 mL of distilled water, followed by both solutions mixed and stirred by a magnet. Afterward, 2 mL of octanoic acid was slowly added to the above solution. Octanoic acid, due to its long hydrocarbon chain and carboxylic acid, can separate the metal cations, thus leading to a homogeneous distribution of particles in the environment. In the next step, a proper amount of NaOH (2 M) was added dropwise to the solution along with continuously vigorous stirring for 2 h. likewise, the solution pH was adjusted to 8–9. During the addition of NaOH to the solution, as soon as the solution became alkaline, the solution color was changed and the precipitate was formed. The suspension was ultrasonically treated for 60 min to form a crystalline phase. The precipitate was collected by Buchner funnel, and next rinsed several times with double distilled

water, and ethanol. Afterward, the dark brown product was placed in the oven at 100 °C for 10 h. Finally, to calcinate the product, it was placed into the furnace at 600 °C for 4 h to remove the organic residual and surfactant.

Synthesis of Hollow Poly (Aniline-co-Pyrrol)

First, Aniline (0.093 g), pyrrole (0.067 g), and TX-100 (0.02 g) were poured into a glass vial containing 20 mL of deionized water, stirred with a magnet for 0.5 h, and then was exposed under ultrasonic irradiation to acquire a uniform solution for another 0.5 h. Afterward, the mixture temperature was kept between 3 to 5 °C for 0.5 h before oxidative polymerization. Subsequently, to start the polymerization process, the APS's aqueous solution (cooled at 3–5 °C) was poured into the aforementioned solution. The above solution was stirred for 30 s to ensure complete mixing, after which the reaction was allowed to proceed with no agitation for 24 h at 3–5 °C. Ultimately, the obtained polymer was filtered off and washed with deionized water until the colorless drain was obtained.

Synthesis of Pt-ZFO/HAP-CH Nanocatalyst

At first, 0.5 mg of hollow poly (aniline-co-pyrrol) was dispersed in 12.5 mL of deionized water. 2 mg of $ZnFe_2O_4$ nanocatalysts was separately added to a container containing 2.5 mL of chitosan solution (1% wt. in acetic acid). Subsequently, they were mixed together and the particles were ultrasonically treated for 1 h to get uniform dispersion. Afterward, 25 µL of $H_2PtCl_6{\cdot}6H_2O$ (1.0 M) was added to the final mixture and stirred for 1 h. Next, 50 µL of the freshly prepared $NaBH_4$ (5.0 M) was poured into the suspension and stirred for 24 h. The final product was centrifuged and washed several times with deionized water. Finally, the catalyst was placed in an oven at 50 °C for 12 h. It was named Pt-ZFO/HAP-CH. Meantime, for comparison, Pt/HAP-CH catalyst was synthesized by the same procedure without utilizing ZFO nanoparticles.

Electrochemical Measurements

All methanol electro-oxidation experiments were performed by a potentiostat/galvanostat Autolab apparatus (PGSTAT 302 N, Metrohm, Netherlands) using a classical three-electrode system at room temperature. A three-electrode cell configuration was utilized, consisting of a Pt rod as an auxiliary electrode, a saturated calomel electrode (SCE) as a reference electrode, and a glassy carbon electrode (GCE, 2 mm diameter) covered with the catalyst as the working electrode. The GCE was polished with Al_2O_3 powder (0.05 mm) before every use. Subsequently, it was cleaned with ethanol and double distilled water and activated by CV technique and applying a potential range between − 1.5 to + 1.5 mV in H_2SO_4 0.5 M (15 repeated cycles). Then, it was coated with catalysts and utilized as the working electrode. The electrocatalyst ink was prepared by dispersing of as-prepared catalyst (2 mg) in 1 mL of chitosan solution by ultrasonication for 10 min. Afterward, 5 µL of the prepared suspension was loaded onto the polished GCE surface and dried naturally to form a uniform thin film at RT.

Electrochemical investigations were performed by cyclic voltammetric, electrochemical impedance spectroscopy, and chronoamperometric techniques at a scan rate of 100 mV/s. The amount of Pt loading on the surface of the modified working electrodes for all the catalysts, measured by ICP-OES was 1.964 µg.

Result and Discussion

Structural Characterizations

Figure 1 shows the FT-IR spectra of (a) octanoic acid, (b) the prepared sample before calcination, and (c) $ZnFe_2O_4$ nanoparticles after calcination. As demonstrated in Fig. 1a, the observed bands in the range of 2650–3450 cm^{-1} are related to the stretching vibration of the O–H band. The band related to the carbonyl group is located at 1718 cm^{-1}. The bending vibrations of CH_3 and CH_2 groups appeared at 1381 and 1461 cm^{-1}, respectively. Two bands at 1220–1330 cm^{-1} and a band at 941 cm^{-1} can be ascribed to the stretching of C–O and out of plane bending of the O–H group, respectively.

As shown in Fig. 1c, the bands observed at 1011 cm^{-1} and 544 cm^{-1} are attributed to (M:metal) M–O stretching and O–M–O bending vibration of $ZnFe_2O_4$, respectively.

The crystalline properties of as-synthesized products were evaluated by XRD analysis, as demonstrated in Fig. 2. The diffraction characteristics peaks at $2\theta = 18.31°$, 30.11°, 35.39°, 42.98°, 53.31°, 56.74°, 62.32°, 70.62°, and 73.65° are corresponded to (111), (220), (311), (400), (422), (511), (440), (620) and (533) facets of the cubic $ZnFe_2O_4$ with the lattice constants $a = b = c = 8.446$ Å (JCPDS no. 04-008-4345), illustrated that the pure $ZnFe_2O_4$ was successfully synthesized [27]. The diffraction peaks at $2\theta = 39.97$, 46.07°, and 67.38° are corresponded to the (111), (200), and (220) planes of Pt nanoparticles, respectively [28]. Debye–Scherrer's equation can be employed to determine the crystallite size of the catalyst [29, 30]. The crystallite size of the Pt and ZFO available in the Pt-ZFO/HAP-CH catalyst were determined 6 nm and 26 nm, respectively.

A crucial analytical tool for the measurement of the magnetic characteristics of nanocatalysts is the vibrating sample magnetometer (VSM), which is broadly utilized for the analysis of magnetic substances. As demonstrated in Fig. 3, the magnetic characteristic of $ZnFe_2O_4$ nanocatalysts was

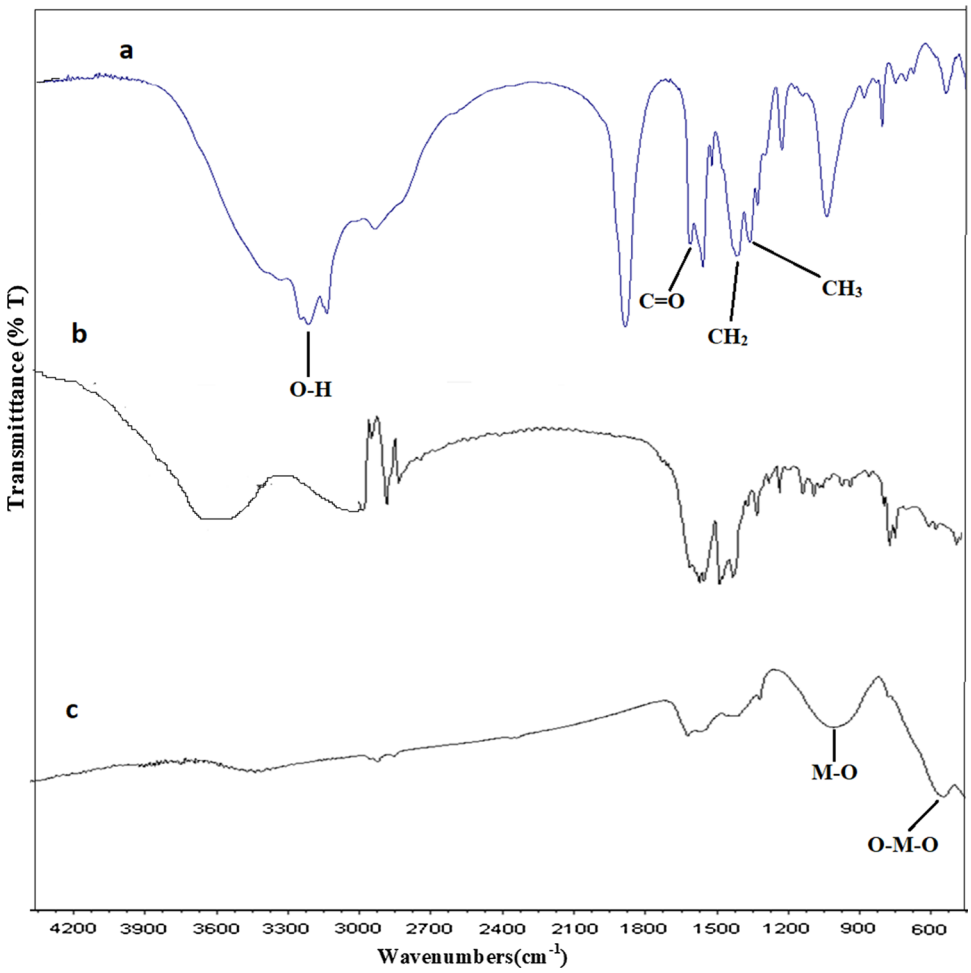

Fig. 1 FT-IR spectra of (a) octanoic acid, (b) the prepared sample before calcination and (c) the prepared sample after calcination

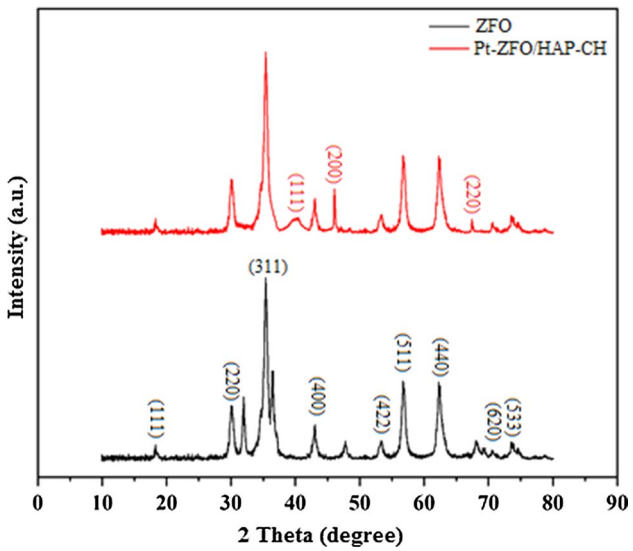

Fig. 2 XRD patterns of the synthesized catalysts

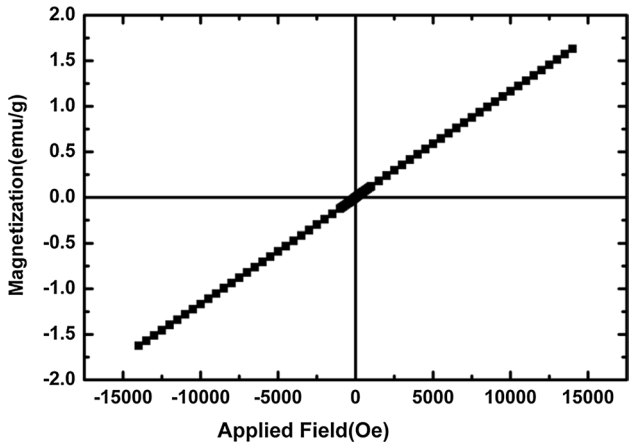

Fig. 3 VSM curve of $ZnFe_2O_4$, measured at room temperature

measured by VSM at room temperature (RT) in the range of ± 15,000 Oe. The VSM profile confirmed that the as-prepared product has paramagnetic characteristics, and the corresponded saturation magnetization value at room temperature is around 1.631 emu/g.

The morphology and structure of the synthesized catalysts were well analyzed by TEM images. TEM images of the prepared HAP, Pt/HAP-CH, and Pt-ZFO/HAP-CH are depicted in Fig. 4. The TEM image of the synthesized HAP is shown in Fig. 4A. The hollow structure is obviously shown. Uniform hollow spheres with an outer diameter of about 100 nm and inner diameter of about 70 nm are observed. TEM image of Pt/HAP-CH is shown in Fig. 4B. The spherical Pt nanoparticles with a mean size of about 5 nm are uniformly dispersed around HAP nanoparticles and CH support. Figure 4C and D show the TEM images of the Pt-ZFO/HAP-CH catalyst. Pt and ZFO nanoparticles are dispersed on HAP-CH support. ZFO nanoparticles have a mean size of 30 nm. Pt nanoparticles are uniformly dispersed on HAP-CH support and also around ZFO nanoparticles. EDX analysis and the elemental mapping of Pt-ZFO/HAP-CH catalyst are shown in Fig. 5.

Electrochemical Studies

To gain comprehensive insights into the relationship between the composition of catalysts and their performance, the cyclic voltammetry experiment was carried out for all the catalysts in 0.5 M H_2SO_4 at a sweep rate of 100 mV/s in the absence of methanol (Fig. 6A). All the catalysts illustrate the standard CV characteristics of Pt-based nanostructures in an acidic solution, consisting of the hydrogen adsorption/desorption current peaks in a low potential region (− 0.33 V to 0.19 V). The electrochemically active surface area (ECSA) of the catalysts can be efficiently measured from the integral value of the areas of the hydrogen adsorption/desorption charge (Q_H) with the following equation (Eq. (1)) [28, 31]:

$$ECSA = \frac{Q_H}{0.21 \times m_{Pt}} \quad (1)$$

m_{Pt} refers to the platinum loading on the surface of the working electrode. Q_H and 0.21 (mC/cm^2) are the overall charge for hydrogen adsorption/desorption and the charge utilized for adsorption of a monolayer of hydrogen on Pt, respectively.

As calculated, Pt-ZFO/HAP-CH is found to have a large ECSA value of 191.562 m^2/g_{Pt}, nearly 1.75 times larger than that of Pt/HAP-CH (109.186 m^2/g_{Pt}) catalyst (Fig. 6B), demonstrating the higher specific surface area of Pt-ZFO/HAP-CH for MOR and more accessible active catalytic of ZFO/HAP-CH to load Pt nanoparticles.

To evaluate the catalytic performance of Pt-ZFO/HAP-CH and Pt/HAP-CH catalysts for methanol electro-oxidation, the CV curves were obtained in an acidic medium (H_2SO_4, 0.5 M) containing methanol 1.03 M at the scan rate of 100 mV/s. As depicted in Fig. 6C, for each CV curve, there are two prevailing characteristic peaks. The first peak in the forward scan (I_f) comes from methanol oxidation, while the second one in the reverse scan (I_b) is associated with the electro-oxidation of the incompletely oxidized carbonaceous species (for example CO) [37].

For Pt-ZFO/HAP-CH catalyst, the first anodic peak is observed at 0.8 V and the second peak in the reverse scan is observed at 0.463 V, whereas for Pt/HAP-CH catalyst, the first and the second peaks of MOR are observed at 0.747 V and 0.419 V, respectively. A very high anodic mass activity of 5775.654 mA/mg $_{Pt}$ is achieved for Pt-ZFO/HAP-CH catalyst, which is much higher than that of Pt/HAP-CH catalyst (3673.297 mA/mg $_{Pt}$).

It should be noted that methanol oxidation occurs on the surface of platinum nanoparticles. Therefore, with an increase in the concentration of platinum nanoparticles, the oxidation of methanol increases, but with an excessive increase in the concentration of platinum nanoparticles, agglomeration of the Pt nanoparticles would happen, which reduces the methanol oxidation. Thus, to determine the catalytic performance of the catalysts and compare it with other synthesized catalysts in the literature, it is better to report the mass activity (mA/mg $_{Pt}$) instead of the current for methanol oxidation in catalysts, as shown in Fig. 6.

Both the ECSA value and the anodic mass activity of Pt-ZFO/HAP-CH are higher than that of Pt/HAP-CH catalyst, evidencing that Pt-ZFO/HAP-CH has remarkably greater catalytic activity towards MOR, compared to Pt/HAP-CH. The better catalytic activity of Pt-ZFO/HAP-CH for MOR is attributed to the presence of ZFO nanoparticles accompanied by Pt nanoparticles and their synergistic effects.

Methanol oxidation occurs on the surface of Pt nanoparticles. The surface oxygen of ZFO nanoparticles would help to remove CO poisoning on the Pt surface. The presence of ZFO nanoparticles improves alcohol oxidation, reduces the formation of carbon monoxide which is the byproduct of methanol oxidation, and facilitates the oxidation of the produced carbon monoxide to carbon dioxide.

Hollow Poly (aniline-co-pyrrole) and chitosan are utilized as support materials for nanoparticles. Chitosan is a biopolymer with a strong affinity for transition metals. The amino group in the chitosan structure is easily protonated in acidic and neutral solutions. Since chitosan is dissolved in a 1% acetic acid aqueous solution, the amino group is protonated to NH_3^+. Therefore, there would be an electrostatic attraction between $PtCl_6^{2-}$ and NH_3^+ with opposite charges which leads to the uniform dispersion of Pt nanoparticles. Furthermore, chitosan causes better adherence of the catalyst ink on the electrode surface. Hollow Poly(aniline-co-pyrrole) can remarkably improve the electron transfer due to its high electrical conductivity and excellent reversible redox behavior (i.e. create the strong hydrogen bonding between the amino and hydroxyl groups of chitosan and amine groups of hollow poly (aniline-co-pyrrole), and also its unique

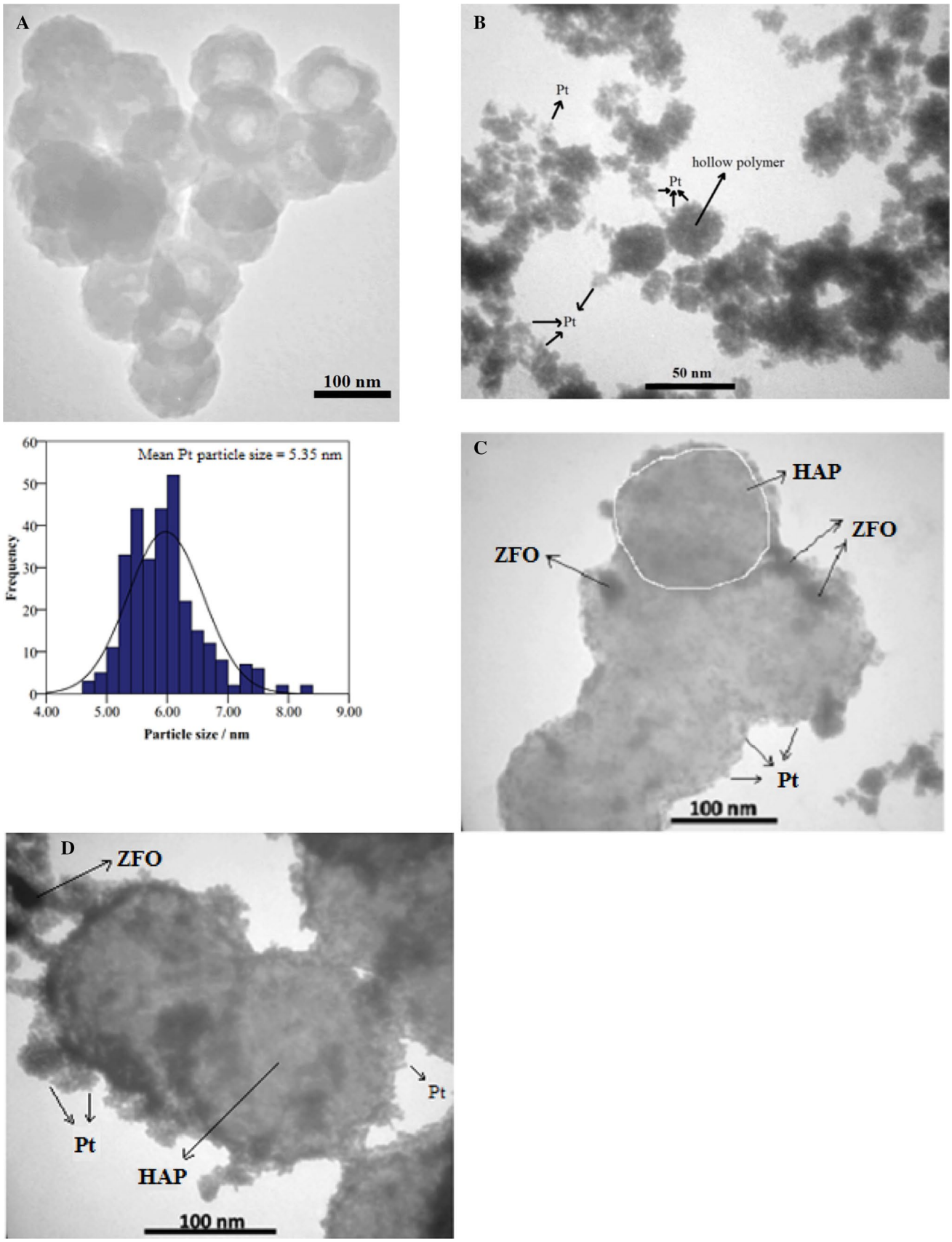

Fig. 4 TEM images of the prepared **A** HAP, **B** Pt/HAP-CH, **C** and **D** Pt-ZFO/HAP-CH

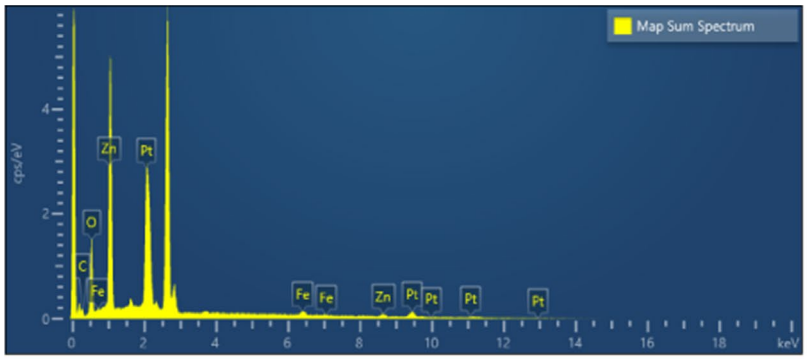

Elements	Weight %	Atomic %
O	22.10	61.05
Fe	1.94	1.53
Pt	43.21	9.79
C	1.83	6.73
Zn	30.92	20.90
Total	100.00	100.00

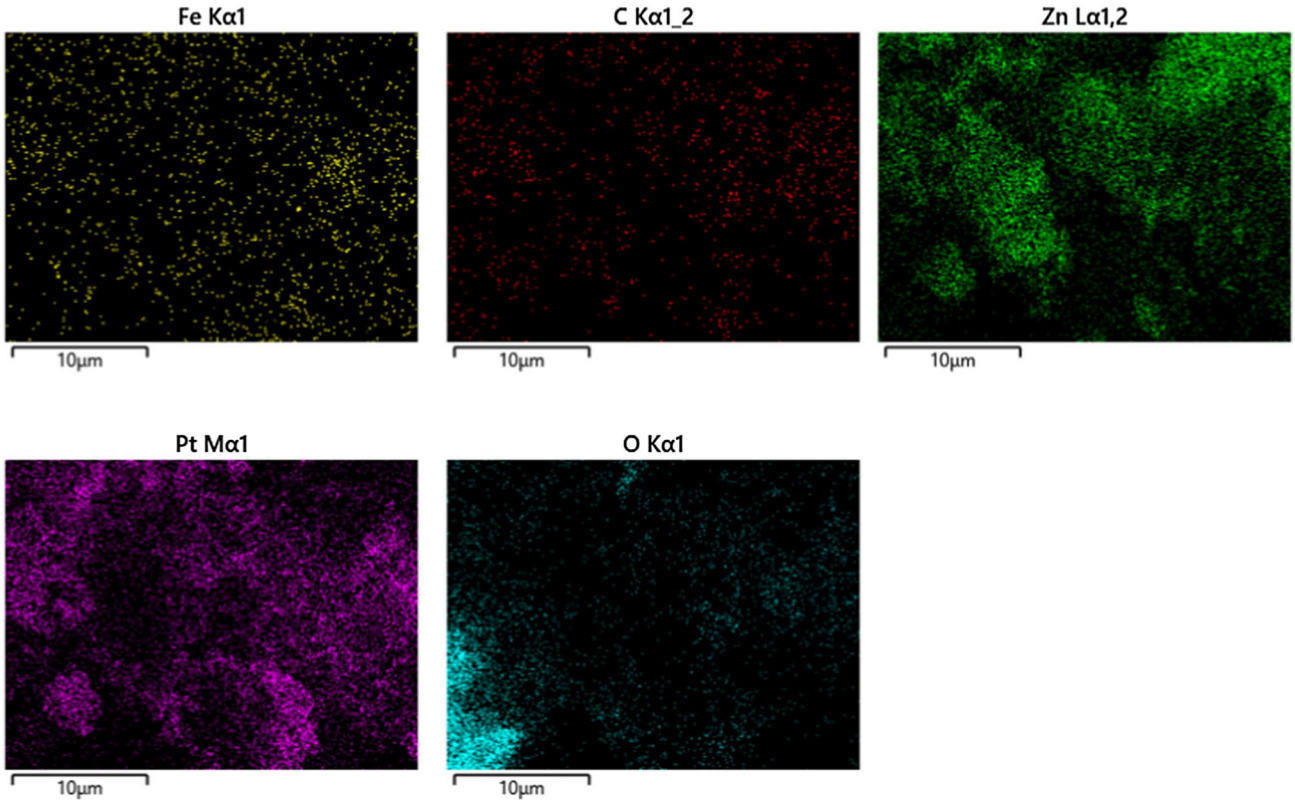

Fig. 5 EDX analysis and the elemental mapping of Pt-ZFO/HAP-CH catalyst

structure and morphology lead to the uniform dispersion of Pt nanoparticles.

The catalytic activity of different Pt-based catalysts for methanol oxidation is demonstrated in Table 1. As can be seen, both fabricated catalysts (Pt-ZFO/HAP-CH and Pt/HAP-CH) have higher mass activity for MOR, compared to the other Pt-based catalysts.

The durability of the catalysts that can be investigated with chronoamperometry (CA) tests is an important factor in assessing their catalytic performance. In this regard, The CA profiles of the synthesized catalysts are evaluated at a constant potential of 0.75 V in H_2SO_4 0.5 M solution containing MeOH 1.03 M vs. SCE. As illustrated in Fig. 6D, at the initial stage of the CA experiment, high mass activities are observed for the synthesized catalysts that are ascribed to the double layer charging and the presence of many active sites for MOR. The mass activity of the synthesized catalysts greatly declined in the first seconds and then reached a steady-state. The primary declines are commonly ascribed to the fact that in the beginning, the active sites are free of the adsorbed methanol molecules and no methanol discharge layer exists around the catalyst, permitting a rapid primary reaction. In the initial seconds, an equilibrium methanol coverage at the surface of the catalyst and methanol equilibrium gradient around the catalysts is established, decreasing the mass activity to a lower value. The progressive decline of

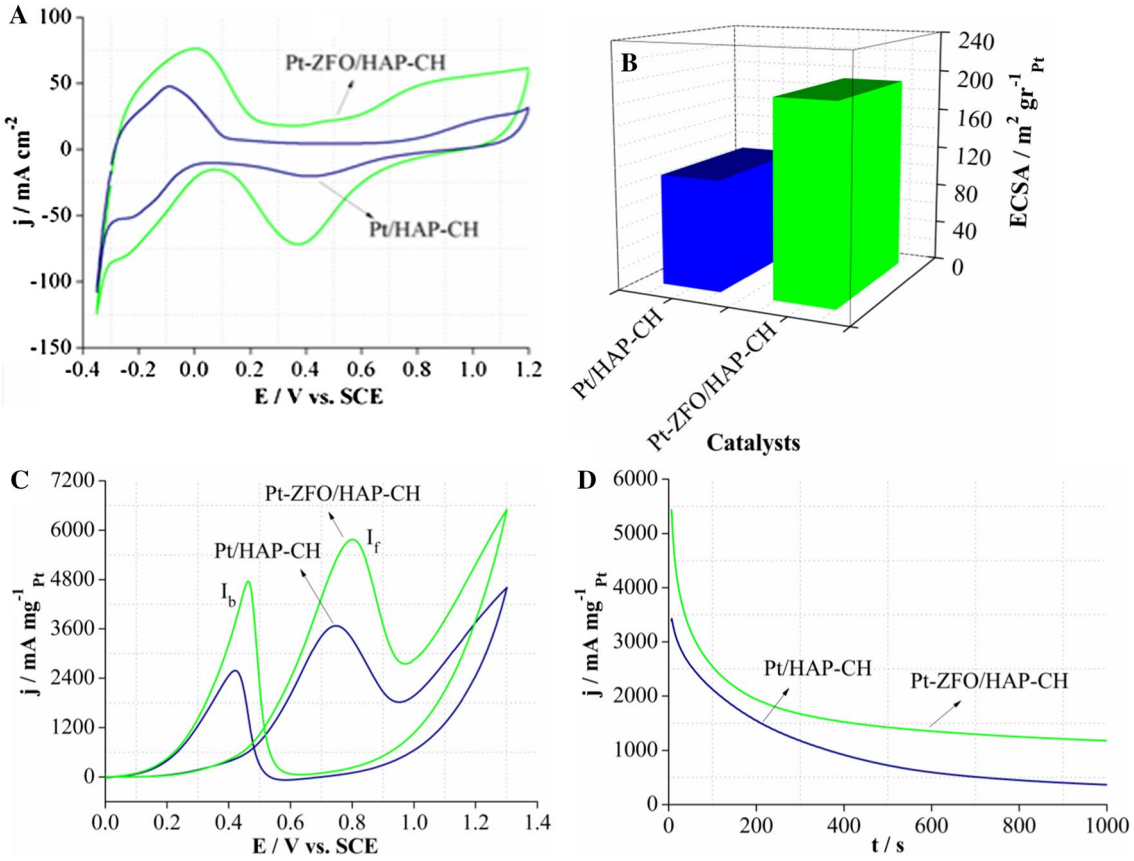

Fig. 6 **A** CV curves of the synthesized catalysts in H_2SO_4 (0.5 M) solution, **B** The ECSA values of the catalysts, **C** CV curves and **D** Chronoamperometric curves of the prepared catalysts for MOR in 0.5 M H_2SO_4 and 1.03 M methanol

Table 1 The catalytic activity of the various Pt-based catalysts for methanol oxidation

Catalyst	Electrolyte concentration (M)	Methanol concentration (M)	Scan rate (mV/s)	Onset potential (V)	Mass activity (mA/mg $_{Pt}$)	Refs
$Pt_1Cu_{0.25}$ ANCs/MWCNTs[a]	0.5	0.5	50	–	1247.3	[32]
Pt_1Cu_2/SN MWCNTs[b]	0.5	0.5	50	–	1589.9	[33]
Pt NDs/Fe-N-S-GR[c]	0.5	0.5	50	0.18	932.7	[34]
Pt/Co-N-S-MWCNT	0.5	0.5	50	0.17	704.9	[35]
Pt HOSs[d]	0.5	0.5	50	0.26	≈490	[36]
Pt-CeO_2 NRs/PA-CH[e]	0.5	1.62	100	0.268	6332.29	[12]
Pt/PVA@NOCC/CH[f]	0.5	1.83	100	0.856	6907.84	[28]
Pt/HAP-CH	0.5	1.03	100	0.09	3673.297	Current study
Pt-ZFO/HAP-CH	0.5	1.03	100	0.08	5775.654	Current study

[a]$Pt_1Cu_{0.25}$ alloy nanoclusters on multi-walled carbon nanotubes

[b]PtCu nanoparticles supported by novel S, N co doped multi walled carbon nanotubes

[c]Pt nanodendrites assembled on Fe, N, and S tri-doped graphene

[d]Pt nanoparticles with hollow-opened structures

[e]Pt-CeO_2 nanorods/polyaniline-chitosan

[f]Pt nanoparticles immobilized on novel electrospun polyvinyl alcohol@Ni/NiO/Cu complex bio-nanofiber/chitosan

the mass activity of catalysts for MOR is most probably associated with the poisoning of the surface of the catalyst that led to the blocking of large active sites on the surface of the catalyst. As can be observed from Fig. 6D, the mass activities of all catalysts gently diminish and get to a pseudo-steady state. This happens because the electrocatalytic reactions maintain an apparent steady-state as adsorption of oxygenated and CO-like species, whereas their redox reactions maintain a relative balance which can be translated as activating the surface via the adsorbed dipolar or anionic species on the surface of the catalysts [38].

Pt-ZFO/HAP-CH had higher stable mass activity for MOR in all times of CA measurements compared to Pt/HAP-CH and demonstrated better tolerance stability towards poisoning carbonaceous species. The results confirmed that Pt-ZFO/HAP-CH had a great catalytic performance for methanol electro-oxidation in acidic media and presented extensive potential applications for DMFCs in the future.

To examine the interfacial characteristics of the surface-modified catalysts, electrochemical impedance spectroscopy (EIS) is utilized. Both the synthesized catalysts exhibit a typical Nyquist plot with a small semicircle in high frequencies, relevant to the charge transfer resistance (R_{ct}), and a line at low-frequencies, related to the diffusion process at the interface of electrolyte and catalysts (Fig. 7A). The Nyquist plots are obtained from 10^4 to 10^{-2} Hz at open circuit potential in the solution of 0.5 M H_2SO_4 and 1.03 M MeOH.

Among the two synthesized catalysts, Pt-ZFO/HAP-CH has a smaller semicircle diameter compared to Pt/HAP-CH, meaning the kinetic reaction rate of electron transfer of methanol dehydrogenation is swifter at this catalyst [39]. The straight line of Pt-ZFO/HAP-CH is steeper than that of Pt/HAP-CH, manifesting its better electrolyte diffusion [40]. FRI studies demonstrate that methanol oxidation reaction is enhanced at Pt-ZFO/HAP-CH catalyst. These outcomes have good agreement with the acquired outcomes from the chronoamperometry and cyclic voltammetry studies of Pt/HAP-CH and Pt-ZFO/HAP-CH catalysts in methanol electro-oxidation.

The effect of methanol concentration on the anodic mass activity of methanol electro-oxidation at Pt/HAP-CH and Pt-ZFO/HAP-CH catalysts was investigated at ambient temperature and 100 mV/s. It sounds that the anodic mass activity of methanol oxidation at both synthesized catalysts increases

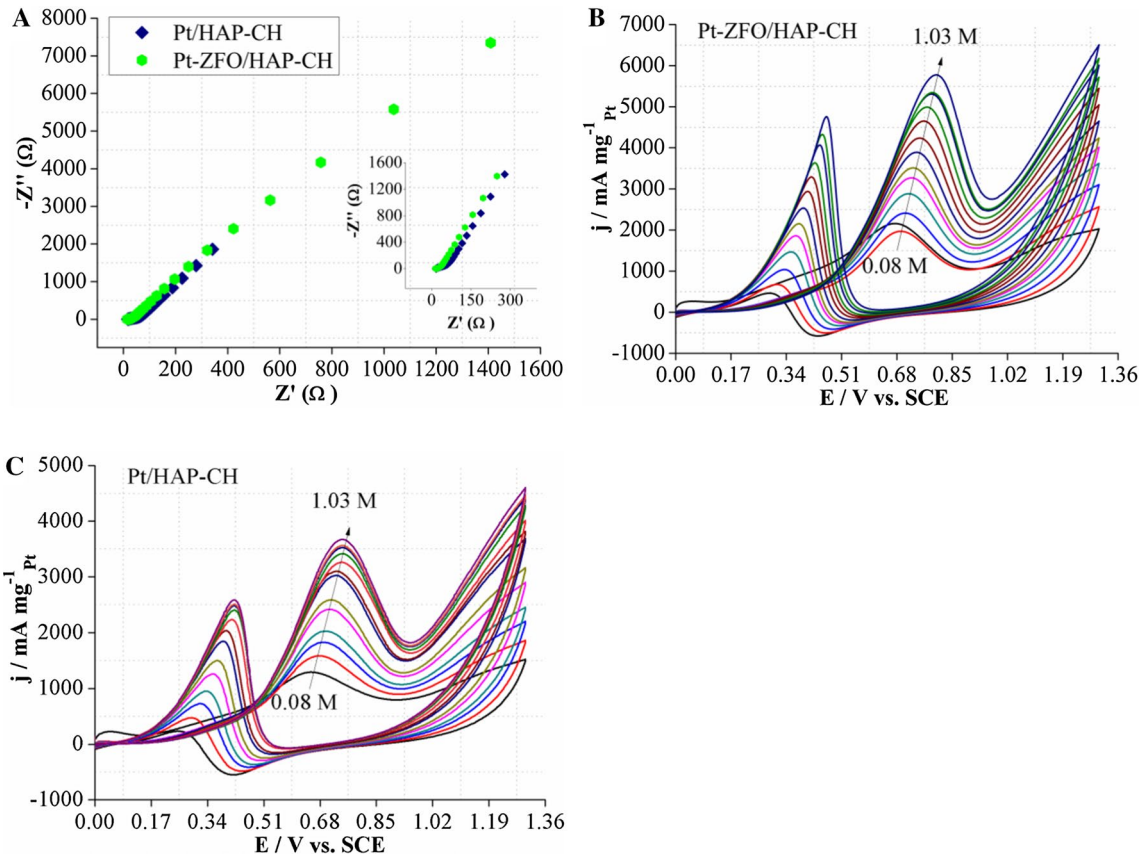

Fig. 7 **A** The EIS Nyquist plots of the catalysts, measured in 1.03 M MeOH + 0.5 M H_2SO_4 at 25 °C, **B** and **C** CV curves for MOR at Pt/HAP-CH and Pt-ZFO/HAP-CH catalysts in 0.5 M H_2SO_4 and various concentration of methanol: (a) 0.08, (b) 0.16, (c) 0.24, (d) 0.32, (e) 0.41, (f) 0.48, (g) 0.56, (h) 0.64, (i) 0.72, (j) 0.79, (k) 0.87, (l) 0.95, (m) 1.03 M

with enhancing the concentration of methanol from 0.08 to 1.03 M. This levels off at methanol concentrations higher than 1.03 M, which is caused by the saturation of the active sites on the electrodes' surface. Moreover, with an increase in the concentration of methanol, the anodic peak potential of MO was shifted to the higher potentials that can be probably ascribed to the enhancement in accumulating the poisonous intermediates on the catalysts' surface with enhancing the methanol concentration. For Pt-ZFO/HAP-CH (Fig. 7B), with an enhancement in methanol concentration from 0.08 to 1.03 M, the mass activity of the anodic MO peak increases from 2157.518 to 5775.654 mA/mg $_{Pt}$. Additionally, by increasing the methanol concentration from 0.08 to 1.03 M at Pt/HAP-CH, the anodic mass activity of the methanol oxidation peak increases from 1289.072 to 3673.297 mA/mg $_{Pt}$ (Fig. 7C).

To verify the impact of scan rate on the catalytic performance of Pt/HAP-CH and Pt-ZFO/HAP-CH catalysts towards methanol oxidation, CV curves were obtained at various scan rates of 30, 60, 90, 100, 130, 160, and 190 mV/s in H_2SO_4 (0.5 M) and methanol (1.03 M) (Fig. 8). As illustrated in Fig. 8, the anodic peak current densities of methanol oxidation on both prepared catalysts were enhanced by increasing the scan rate. In addition, for both synthesized catalysts, there is a linear correlation between the anodic current density of the MO peak and the square root of scan rate ($\upsilon^{0.5}$) which confirms that methanol oxidation is controlled by the diffusion of methanol from the solution to the electrode surface [41].

Conclusion

This research aimed to synthesize a novel catalyst with enhanced catalytic performance towards methanol electrooxidation. Hollow poly (aniline-co-pyrrol) was synthesized and utilized accompanied by chitosan as support for Pt nanoparticles. ZFO nanoparticles were synthesized and used accompanied by Pt nanoparticles to prepare the novel Pt-ZFO/HAP-CH. The electrochemical behavior of Pt-ZFO/HAP-CH was investigated towards methanol oxidation and compared with that of Pt/HAP-CH. The results revealed that Pt-ZFO/HAP-CH catalyst had higher mass activity, higher ECSA, better durability, reduced charge transfer resistance,

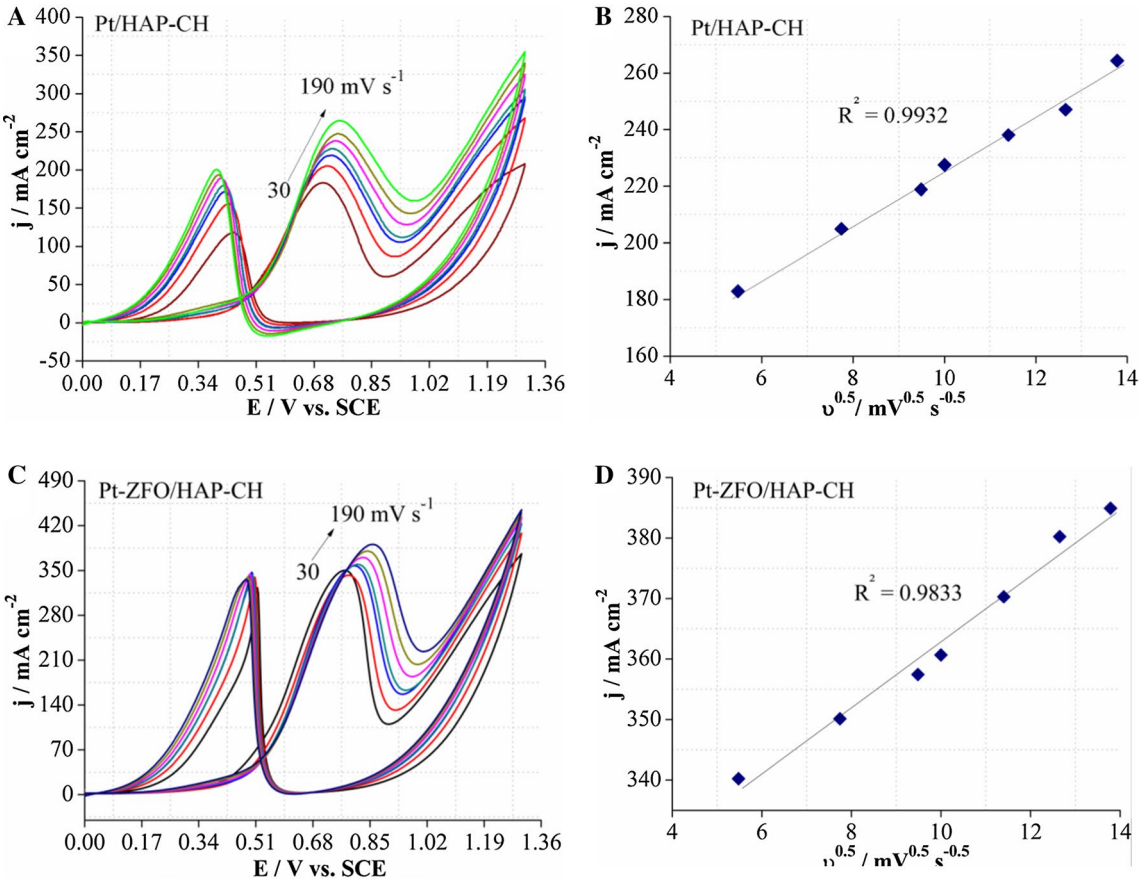

Fig. 8 CV curves of the prepared catalysts in 0.5 M H_2SO_4 and 1.03 M methanol at different scan rates of 30, 60, 90, 100, 130, 160, and 190 mV/s. The plots of j vs. $\upsilon^{0.5}$ of the catalysts are also shown

and better electrical conductivity for MOR compared to Pt/HAP-CH. The excellent catalytic performance of Pt-ZFO/HAP-CH for methanol electro-oxidation is attributed to the synergistic effect of ZFO nanoparticles accompanied by Pt nanoparticles and very uniform dispersion of Pt nanoparticles on HAP-CH support and around ZFO nanoparticles. Pt-ZFO/HAP-CH can be used as a promising catalyst for application in DMFCs.

Acknowledgements We acknowledge Esfarayen University of Technology, Zahedan Branch, Islamic Azad University, and Science and Research Branch, Islamic Azad University of Tehran for their financial supports.

References

1. S. M. Mostashari, R. A. Dehkharghani, F. Afshar-Taromi, and M. Farsadrooh (2021). *Int. J. Hydrogen Energy* **46**, 9406.
2. G. Sreenivasa Kumar, N. Ramamanohar Reddy, B. Sravani, L. Subramanyam Sarma, T. Veera Reddy, V. Madhavi, and S. Adinarayana Reddy (2021). *J. Clust. Sci.* **32**, 27.
3. M.-S. Ekrami-Kakhki, A. Naeimi, and F. Donyagard (2019). *Int. J. Hydrogen Energy* **44**, 1671.
4. F. Hong, M. Wang, and Y. Ni (2018). *J. Clust. Sci.* **29**, 663.
5. M. Ghanbari, G. H. Rounaghi, N. Ashraf, M. Paydar, I. Razavipanah, and M. Karimi-Nazarabad (2017). *J. Clust. Sci.* **28**, 2133.
6. J. Li, Z. Luo, Y. Zuo, J. Liu, T. Zhang, P. Tang, J. Arbiol, J. Llorca, and A. Cabot (2018). *Appl. Catal. B: Environ.* **234**, 10.
7. J. Abrego-Martínez, Y. Wang, A. Moreno-Zuria, Q. Wei, F. Cuevas-Muniz, L. Arriaga, S. Sun, and M. Mohamedi (2019). *Electrochim. Acta* **297**, 230.
8. S. Yang, C. Hu, D. Liu, T. Zhang, T. Guo, and F. Liao (2014). *J. Clust. Sci.* **25**, 337.
9. D. Van Dao, G. Adilbish, T. D. Le, T. T. Nguyen, I.-H. Lee, and Y.-T. Yu (2019). *J. Catal.* **377**, 589.
10. R. Chang, L. Zheng, C. Wang, D. Yang, G. Zhang, and S. Sun (2017). *Appl. Catal. B: Environ.* **211**, 205.
11. Y. Kang, Q. Xue, P. Jin, J. Jiang, J. Zeng, and Y. Chen (2017). *ACS Sustain. Chem. Eng.* **5**, 10156.
12. M.-S. Ekrami-Kakhki, S. Pouyamanesh, S. Abbasi, G. Heidari, and H. Beitollahi (2021). *J. Clust. Sci.* **32**, 363.
13. P. Yang, R. Devasenathipathy, W. Xu, Z. Wang, D.-H. Chen, X. Zhang, Y. Fan, and W. Chen (2021). *ACS Appl. Nano. Mater.* **4**, 10584.
14. H. Shi, F. Liao, W. Zhu, C. Shao, and M. Shao (2020). *Int. J. Hydrogen Energy* **45**, 16071.
15. B. Makiabadi, M.-S. Ekrami-Kakhki, N. Farzaneh, and S. Abbasi (2017). *J. Mater. Sci.: Mater. Electron.* **28**, 12373.
16. M. Farsadrooh, J. Torrero, L. Pascual, M. A. Peña, M. Retuerto, and S. Rojas (2018). *Appl. Catal. B: Environ.* **237**, 866.
17. Z. Li, X. Jiang, X. Wang, J. Hu, Y. Liu, G. Fu, and Y. Tang (2020). *Appl. Catal. B: Environ.* **277**.
18. X. Bai, J. Geng, S. Zhao, H. Li, and F. Li (2020). *ACS Appl. Mater. Interfaces* **12**, 23046.
19. Z. Shen, X. Wang, B. Luo, and L. Li (2015). *J. Mater. Chem. A* **3**, 18146.
20. Q. Lin, A. Armin, P. L. Burn, and P. Meredith (2016). *Acc. Chem. Res.* **49**, 545.
21. A. Galal, N. F. Atta, and M. A. Hefnawy (2020). *Synth. Met.* **266**.
22. M. Noroozifar, M. Khorasani-Motlagh, R. Khaleghian-Moghadam, M.-S. Ekrami-Kakhki, and M. Shahraki (2013). *J. Solid State Chem.* **201**, 41.
23. B. Wu, W. Zhao, L. Hou, T. Zhang, and C. Yang (2017). *J. Clust. Sci.* **28**, 1295.
24. M. Nasrollahzadeh, M. Jahanshahi, M. Yaldagard, and M. Salehi (2018). *Bull. Mater. Sci.* **41**, 1.
25. S. Eris, Z. Daşdelen, Y. Yıldız, and F. Sen (2018). *Int. J. Hydrogen Energy* **43**, 1337.
26. M.-S. Ekrami-Kakhki, N. Farzaneh, S. Abbasi, H. Beitollahi, and S. A. Ekrami-Kakhki (2018). *Electron. Mater. Lett.* **14**, 616.
27. A. Mehrani and K. Mehrani (2012). *J. Inorg. Organomet. Polym.* **22**, 1419.
28. A. Naeimi, M.-S. Ekrami-Kakhki, and F. Donyagard (2021). *Int. J. Hydrogen Energy* **46**, 18949.
29. S. M. Mostashari, R. A. Dehkharghani, M. Farsadrooh, and F. Afshar-Taromi (2022). *J. Mol. Liq.* **360**.
30. M. Hajnajafi, A. Khorshidi, M. Farsadrooh, and A. G. Gilani (2021). *Energy Fuels* **35**, 3396.
31. M.-S. Ekrami-Kakhki, N. Farzaneh, and E. Fathi (2017). *Int. J. Hydrogen Energy* **42**, 21131.
32. J. Zhong, L. Li, M. Waqas, X. Wang, Y. Fan, J. Qi, B. Yang, C. Rong, W. Chen, and S. Sun (2019). *Electrochim. Acta* **322**.
33. J. Zhong, K. Huang, W. Xu, H. Tang, M. Waqas, Y. Fan, R. Wang, and W. Chen (2021). *Chin. J. Catal* **42**, 1205.
34. J.-P. Zhong, C. Hou, L. Li, M. Waqas, Y.-J. Fan, X.-C. Shen, W. Chen, L.-Y. Wan, H.-G. Liao, and S.-G. Sun (2020). *J. Catal.* **381**, 275.
35. J. Zhong, M. Sun, S. Xiang, Y. Fan, M. Waqas, K. Huang, Y. Tang, W. Chen, and J. Yang (2020). *Appl. Surf. Sci.* **511**.
36. X. Wang, M. Sun, S. Xiang, M. Waqas, Y. Fan, J. Zhong, K. Huang, W. Chen, L. Liu, and J. Yang (2020). *Electrochim. Acta* **337**.
37. M. Khorasani-Motlagh, M. Noroozifar, and M.-S. Ekrami-Kakhki (2011). *Int. J. Hydrogen Energy* **36**, 11554.
38. M. Farsadrooh, M. Z. Yazdan-Abad, M. Noroozifar, H. Javadian, N. Alfi, and A. R. Modarresi-Alam (2020). *Int. J. Hydrogen Energy* **45**, 27312.
39. Z. Gu, S. Li, Z. Xiong, H. Xu, F. Gao, and Y. Du (2018). *J. Colloid Interface Sci.* **521**, 111.
40. K. Kakaei, A. Rahimi, S. Husseindoost, M. Hamidi, H. Javan, and A. Balavandi (2016). *Int. J. Hydrogen Energy* **41**, 3861.
41. Y. Zhao, R. Wang, Z. Han, C. Li, Y. Wang, B. Chi, J. Li, and X. Wang (2015). *Electrochim. Acta* **151**, 544.